JOURNAL OF SCIENCE AND TECHNOLOGY
ISSN: 2229-8460 e-ISSN: 2600-7924

JST

Vol. 16 No. 2 (2024) 85-95
https://publisher.uthm.edu.my/ojs/index.php/jst

Mathematical Modelling of Bödewadt Flow in Nanofluid: Implications of Velocity Slip and Thermal Slip Over a Stretching Disk

Lim Ming Hui[1], Lok Yian Yian[1]*

[1] *Mathematics Section, School of Distance Education, Universiti Sains Malaysia, 11800 USM Penang, MALAYSIA*

*Corresponding Author: lokyy@usm.my
DOI: https://doi.org/10.30880/jst.2024.16.02.010

Article Info

Received: 2 October 2024
Accepted: 17 November 2024
Available online: 21 November 2024

Keywords

Bödewadt flow, velocity slip, thermal slip, nanofluid, stretching disk, numerical solutions

Abstract

This paper investigates the flow and heat transfer attributes of Bödewadt flow in nanofluid, accounting for velocity slip, thermal slip, and a radially stretching permeable disk. The von Kármán similarity variables have been applied to simplify the governing partial differential equations into nonlinear ordinary differential equations, which are subsequently solved numerically using Python's solve_bvp module. The results indicate that an adequate amount of stretching rate is required for the heat transfer equation's similarity solution to be present in the case of a no-slip stretching disk in order to satisfy the boundary conditions. The momentum and thermal boundary layer thickness are affected by the presence of velocity slip and thermal slip, along with stretching parameter. Additionally, variation of the local skin friction coefficient and local Nusselt number shows that heat transfer enhancement occurs in optimal situations when the slip value is minimal, a higher volume fraction of nanoparticles is used, and larger stretching parameters are applied.

1. Introduction

The heat transfer process is a crucial aspect of many industrial applications, particularly for cooling equipment. Enhancing heat transfer efficiency continues to be a primary goal for product developers. Nanofluids, which contain nanoparticles in base fluids such as water or ethylene glycol, have garnered considerable interest for their exceptional thermal characteristics. Nanoparticles increase the thermal conductivity of the fluid, making nanofluids very efficient for heat transfer purposes. Metals and metal oxides nanoparticles are commonly used for their excellent conductive and convective properties.

The idea of nanofluids, initially introduced by Choi and Eastman [1], has shown promise in improving heat transfer efficiency compared to conventional fluids. The presence of nanoparticles in the base fluid will impact the thermophysical characteristics of the fluid, including density, viscosity, thermal conductivity, and heat transfer coefficient. The effectiveness of heat transfer with nanofluids is influenced by the volume concentration, material, and size of the nanoparticles. Frequently used nanoparticles are copper, silver, copper oxide, and titanium dioxide. In addition, the mixture of different nanoparticles in hybrid nanofluids provides more opportunities to improve heat transfer.

Bödewadt flow is a fluid that rotates at a constant angular velocity while being a certain distance away from a disk that is not in motion. Bödewadt [2] had successfully obtained the exact solutions of the Bödewadt flow for the Navier-Stokes equation with no-slip condition. Bödewadt flow causes friction near the disk surface, leading to

a secondary flow moving inward radially and upward axially. The pattern of this rotating flow can be described as the "teacup effect" [3].

Studies on the Bödewadt flow and heat transfer in fluids exhibiting Newtonian behaviour have highlighted several crucial aspects. Rahman and Andersson [4], and Rafiq and Hashmi [5] concluded that the role of suction is crucial in obtaining similarity solutions, resulting in a decrease in the thickness of the thermal boundary layer due to the enhanced suction. The stretching of a stationary disk influences both momentum and thermal boundary layers, requiring either adequate wall permeability or a sufficient stretching rate for a meaningful temperature profile, as studied by Turkyilmazoglu [6]. Slip conditions significantly influence the velocity field, as the increased slip effect decreases the torque necessary to keep the disk stationary [7]. Rahman and Andersson [8] studied the interaction of fluid-particle suspension and found that suction conditions can strengthen the spiralling particle motion and reduce the revolving fluid motion. Besides, an entropy generation analysis done by Mustafa et al. [9] on Bödewadt flow and heat transfer under strong wall suction conditions revealed a new mechanism called as nonlinear radiation. On the other hand, research on Bödewadt flow and heat transfer in fluids exhibiting non-Newtonian behaviour, particularly the Reiner-Rivlin fluid, has shown that slip conditions significantly affect velocity and temperature fields [10]. Suction and injection have been found to influence the boundary layer thickness and velocity profile oscillations [11]. The momentum and thermal boundary layers are impacted by the stretching and shrinking of a disk [12].

Some studies on Bödewadt flow have focused on nanofluids, while some researchers exploring hybrid nanofluids. The goal of using nanofluids is to enhance heat transfer efficiency. Mustafa et al. [13] discovered that the skin friction coefficient and heat transfer rate enhance by increasing the volume fraction of nanoparticles in the scenario of a stretching disk with no slip conditions. However, Mahyuddin et al. [14] discovered that heat transfer is improved only when using a smaller number of nanoparticles in the presence of significant suction, where this finding was subsequently confirmed by Abbas et al. [15]. In the context of Ferrofluids, according to Joshi et al. [16], enhancing the heat transfer rate can be achieved by increasing the porosity of the porous medium and rotating the nanofluid with ferromagnetic particles. Hani et al. [17] applied a Bayesian approach to analyse the hydromagnetic Bödewadt flow of Casson nanofluid over a stretching disk, uncovering relationships among different parameters. It has been discovered that thermal radiation enhances heat transport in a magnetic nanofluid of porous medium [18]. A study by Rauf et al. [19] found that the Hall current in hybrid nanofluid increases radial velocity and decreases axial velocity in Bödewadt flow. Pandey and Das [20] examined the thermodynamic behaviour of Bödewadt hybrid-nanofluid flowing over a permeable disk under the influence of a magnetic field. Horizontal magnetic field has a more notable impact than vertical magnetic field, according to their findings. All previous research employed the Tiwari and Das model for nanofluid representation, except for a study by Khan et al. [21] that utilized the Buongiorno model. Khan et al. [21] observed an oscillatory decaying pattern on the velocity components when the disk is not stretching.

The goal of this paper is to study the effects of velocity slip and thermal slip on the Bödewadt flow in nanofluid over a radially stretched disk. This type of flow is commonly used in mechanical rotor-stator system, turbo-machinery, vortex chambers, and chemical mixing in chemical engineering [22]. The slip condition is important when dealing with fluids that contain particles or suspensions. According to Shafiq et al. [23], slip conditions in nanofluids can decrease the heat and mass transfer rates, but the impacts of velocity slip and thermal slip of the stretching disk on Bödewadt flow in nanofluids are still not completely clear. The problem's mathematical model includes the continuity equation, momentum equation, and energy equation. These are obtained from the fundamental principles of mass conservation, Newton's second law, and the first law of thermodynamics. By utilizing an appropriate similarity transformation, the governing equations were effectively transformed into nonlinear ordinary differential equations. Numerical solutions for important parameters such as slip and stretching parameters, are examined to see how they impact flow and heat transfer properties. It has to be mentioned here that the Bödewadt slip flow on a convectively heated porous disk in nanofluid was analysed by Rafiq et al. [24], while Abbas et al. [15] investigated the problem with temperature jump. Both studies considered the effects of slip condition over a permeable disk but not stretching disk.

2. Mathematical Formulation

Consider an incompressible Bödewadt flow in nanofluid over a stretching disk. Assume that the flow is rotating at a steady angular speed Ω at a distance away from the stationary disk. The disk is radially and linearly stretched out from its origin. Figure 1 visualize the physical model and coordinate system of this problem. The basic equations that govern Bödewadt flow in cylindrical coordinates (r, φ, z) are given as follows [4, 13, 14]:

J. of Science and Technology Vol. 16 No. 2 (2024) p. 85-95

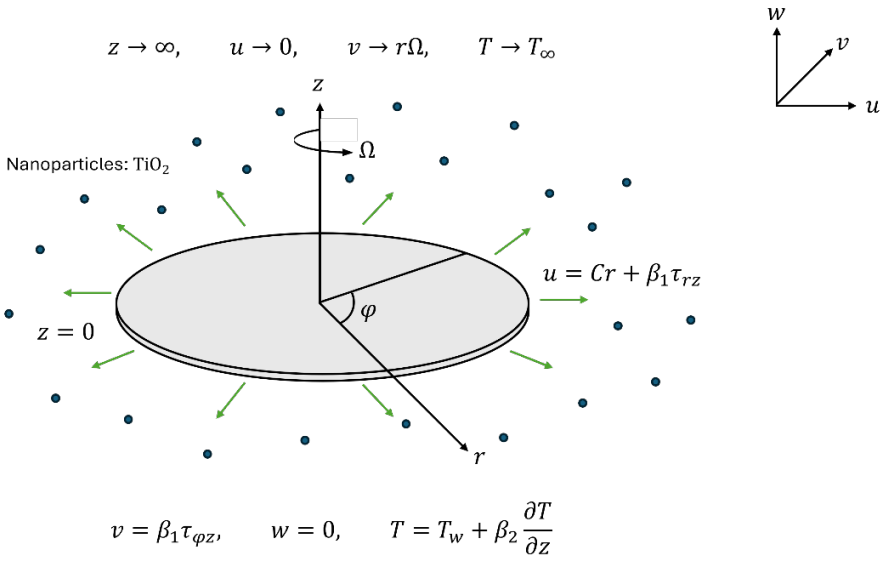

Fig. 1 *The physical model and coordinate system*

$$\frac{\partial u}{\partial r} + \frac{u}{r} + \frac{\partial w}{\partial z} = 0, \tag{1}$$

$$u\frac{\partial u}{\partial r} - \frac{v^2}{r} + w\frac{\partial u}{\partial z} = -\frac{1}{\rho_{nf}}\frac{\partial p}{\partial r} + \nu_{nf}\left(\frac{\partial^2 u}{\partial r^2} + \frac{1}{r}\frac{\partial u}{\partial r} - \frac{u}{r^2} + \frac{\partial^2 u}{\partial z^2}\right), \tag{2}$$

$$u\frac{\partial v}{\partial r} + \frac{uv}{r} + w\frac{\partial v}{\partial z} = \nu_{nf}\left(\frac{\partial^2 v}{\partial r^2} + \frac{1}{r}\frac{\partial v}{\partial r} - \frac{v}{r^2} + \frac{\partial^2 v}{\partial z^2}\right), \tag{3}$$

$$u\frac{\partial w}{\partial r} + w\frac{\partial w}{\partial z} = -\frac{1}{\rho_{nf}}\frac{\partial p}{\partial z} + \nu_{nf}\left(\frac{\partial^2 w}{\partial r^2} + \frac{1}{r}\frac{\partial w}{\partial r} + \frac{\partial^2 w}{\partial z^2}\right), \tag{4}$$

$$u\frac{\partial T}{\partial r} + w\frac{\partial T}{\partial z} = \alpha_{nf}\left(\frac{\partial^2 T}{\partial r^2} + \frac{1}{r}\frac{\partial T}{\partial r} + \frac{\partial^2 T}{\partial z^2}\right), \tag{5}$$

where (u, v, w) represent the velocity in radial, azimuthal and axial directions, respectively, T is the temperature, ρ is the density, p is the pressure, ν is the kinematic viscosity, and α is the thermal diffusivity. The subscript nf represents the nanofuid. The above governing equations can be further simplified when applying the boundary layer theory approximation and order of magnitude analysis. Moreover, the rotation around the z-axis for axisymmetric flow has led to the exclusion of the derivative with respect to the azimuthal coordinate (φ).

The boundary conditions are outlined as below,

$$\begin{aligned} u = Cr + \beta_1 \tau_r, \quad v = \beta_1 \tau_\varphi, \quad w = 0, \quad T = T_w + \beta_2 \frac{\partial T}{\partial z}, \quad \text{at } z = 0, \\ u \to 0, \quad v \to r\Omega, \quad T \to T_\infty \quad \text{as } z \to \infty, \end{aligned} \tag{6}$$

where $C > 0$ is the stretching rate, β_1 is the velocity slip, β_2 is the thermal slip, T_w is the constant temperature at the disk surface and T_∞ is the constant ambient temperature at the far-field region. The radial stress (τ_r) and tangential stress (τ_φ) is expressed as

$$\tau_r = \mu_{nf}\frac{\partial u}{\partial z}, \qquad \tau_\varphi = \mu_{nf}\frac{\partial v}{\partial z}. \tag{7}$$

The mathematical expressions for the characteristics of nanofluids, including density, heat capacity, dynamic viscosity, kinematic viscosity, thermal diffusivity, thermal conductivity and pressure terms are given as follows [15]:

$$\frac{\rho_{nf}}{\rho_f}=\frac{\rho_s}{\rho_f}\phi+1-\phi,\qquad \frac{(\rho C_p)_{nf}}{(\rho C_p)_f}=\frac{(\rho C_p)_s}{(\rho C_p)_f}\phi+1-\phi,\qquad \frac{\mu_{nf}}{\mu_f}=\frac{1}{(1-\phi)^{2.5}},\qquad \alpha_{nf}=\frac{k_{nf}}{(\rho C_p)_{nf}},$$

$$v_{nf}=\frac{\mu_{nf}}{\rho_{nf}},\qquad \frac{k_{nf}}{k_f}=\frac{\left(\frac{k_s+2k_f}{k_f-k_s}\right)-2\phi}{\left(\frac{k_s+2k_f}{k_f-k_s}\right)+2\phi},\qquad \frac{p}{\rho_{nf}}=-\frac{1}{2}w^2+\nu_{nf}\frac{\partial w}{\partial z}+\frac{1}{2}r^2\Omega^2, \tag{8}$$

where the subscript f and s denote base fluid and nanoparticle, respectively. The nanoparticle's volume fraction is defined as ϕ.

We now introduce the von Kármán transformation [14, 15]:

$$u(r,z)=r\Omega F(\eta),\quad v(r,z)=r\Omega G(\eta),\quad w(r,z)=\sqrt{\nu_f\Omega}H(\eta),\quad T(r,z)=T_\infty+(T_w-T_\infty),\ \theta(\eta),\eta=z\sqrt{\Omega/\nu_f}. \tag{9}$$

Using similarity variables (9) to the governing equations (1)-(5) led to a set of coupled ordinary differential equations and boundary conditions:

$$H'=-2F, \tag{10}$$

$$F''=A(1+HF'+F^2-G^2), \tag{11}$$

$$G''=A(H\mathrm{G}'+2FG), \tag{12}$$

$$\theta''=B(PrH\theta'), \tag{13}$$

where $A=\left[(1-\phi)^{2.5}\left(1-\phi+\phi\frac{\rho_s}{\rho_f}\right)\right]$, $B=\left[\frac{1-\phi+\phi\,(\rho c_p)_s/(\rho c_p)_f}{k_{nf}/k_f}\right]$, $Pr=\nu_f/\alpha_f$ is the Prandtl number of the base fluid. The Prandtl number of water is assumed to be around 6.2 – 6.9.

The boundary conditions (6) now become

$$H(0)=0,\qquad F(0)=\lambda+S_1F'(0),\qquad G(0)=S_1G'(0),\qquad \theta(0)=1+S_2\theta'(0),$$
$$F\to 0,\qquad G\to 1,\qquad \theta\to 0,\qquad \text{as}\ \ \eta\to\infty. \tag{14}$$

In this case, $S_1=\beta_1\mu_{nf}$ represents the velocity slip parameter, $S_2=\beta_2\sqrt{\frac{\Omega}{\nu_f}}$ represents the thermal slip parameter, and $\lambda=\frac{c}{\Omega}(>0)$ represents the stretching parameters as the proportion of stretching rate to the rotation rate.

This study considered nanoparticles of titanium dioxide (TiO_2) dispersed in water as the fluid medium. Furthermore, the flow and heat transfer characteristics for TiO_2 nanoparticles have been compared with those for Copper (Cu). TiO_2 is categorized as metal oxide, and Cu is an example of metal, they are commonly used as nanoparticles. The thermophysical properties of both the base fluid and nanoparticles are provided in Table 1.

Table 1 *The thermophysical properties [25, 26]*

Properties	Base Fluid	Nanoparticles	
	Water	Cu	TiO_2
Thermal conductivity, k (W/mK)	0.613	401	8.9538
Density, ρ (kg/m^3)	997.1	8933	4250
Specific heat capacity, C_p (J/kg K)	4179	385	686.2

The skin friction coefficient and the Nusselt number are crucial in examining the flow and heat transfer properties. The definition of the skin friction coefficient is as follows:

$$C_f=\frac{\sqrt{\tau_r^2+\tau_\varphi^2}}{\rho_f(r\Omega)^2}, \tag{15}$$

where τ_r and τ_φ are defined by Eq. (7).

By using the similarity transformation (9) and the boundary conditions (14), the local skin friction coefficient (15) can be rewritten as

J. of Science and Technology Vol. 16 No. 2 (2024) p. 85-95

$$Re_r^{1/2} C_f = \frac{\sqrt{G'(0)^2 + F'(0)^2}}{(1-\phi)^{2.5}}, \tag{16}$$

where $Re_r = \frac{r\Omega^2}{v_f}$ is the local Reynolds number.

The definition of the Nusselt number is as follows:

$$Nu_r = \frac{rq_w}{(T_w - T_\infty)k_f}. \tag{17}$$

Here, q_w refers to the heat flux from the disk,

$$q_w = -k_{nf} \left.\frac{\partial T}{\partial z}\right|_{at\ z=0}. \tag{18}$$

Using the similarity transformation (9), boundary conditions (14) and heat flux (17), the local Nusselt number can be rewritten as

$$Re_r^{-1/2} Nu_r = -\frac{k_{nf}}{k_f}\theta'(0). \tag{19}$$

This study involves four crucial parameters: the stretching parameter, λ, the velocity slip parameter, S_1, and the thermal slip parameter, S_2 as well as the Prandtl number, Pr.

3. Numerical Results and Discussions

The solve_bvp module from Python scipy.integrate library was used to solve the coupled ordinary differential equations (10)-(13) subject to the boundary conditions (14). In this module, a fourth-order collocation algorithm with residual error control is employed. A damped Newton method, with an affine-invariant criterion function, is used to solve the system [27]. The computation utilized a boundary layer thickness of 16 and a grid size of 0.001 in η The boundary layer thickness value is selected to be large enough to ensure that the numerical solutions obtained meet the terminal boundary conditions. As commented by Andersson [28] and Pantokratoras [29], a wider calculation domain should be used to obtain accurate numerical solution. On the other hand, the grid size in η has been examined and it is found that reducing the value of $\delta\eta$ below 0.001 would not change the obtained numerical solutions, hence, the optimum grid size in η is 0.001. This study selected TiO_2 nanoparticles and water as the primary fluid to produce a nanofluid. The error tolerance was established at 1×10^{-7}. The Prandtl number used in this study is $Pr = 6.2$ for water.

Validation of the numerical program's results is performed to ensure its accuracy. Table 2 shows the comparison between current findings and the results acquired by Mahyuddin et al. [14] and Mustafa et al. [13] (the Keller-box method), as well as Turkyilmazoglu [6] (Chebyshev collocation method). The validation is also done by computing some results for copper nanoparticles and then compared with those obtained by Mahyuddin et al. [14]. In short, the validation results obtained using Python's solve_bvp module are acceptable and the program code is verified as correct.

Table 2 *Comparison of the numerical findings with the results that have been previously reported when* $\phi = S_1 = S_2 = 0, Pr = 1$ *with different values of* λ

λ		$-F'(0)$	$G'(0)$	$-\theta(0)$	$-H(\infty)$
1	Current – solve_bvp	1.865469	0.685170	0.543288	0.469717
	Mahyuddin et al. [14]	1.865469	0.685170	0.547181	0.469714
	Mustafa et al. [13]	1.865469	0.685170	0.547181	0.469713
	Turkyilmazoglu [6]	1.865469	0.685170	0.543080	0.469350
5	Current – solve_bvp	13.466234	1.200076	1.883582	3.215196
	Mahyuddin et al. [14]	13.466235	1.200076	1.883582	3.215196
	Mustafa et al. [13]	13.466230	1.200076	1.883582	3.215196
	Turkyilmazoglu [6]	13.466230	1.200076	1.883582	3.215196
10	Current – solve_bvp	37.360360	1.678167	2.686657	4.700369
	Mahyuddin et al. [14]	37.360366	1.678166	2.686657	4.700371
	Mustafa et al. [13]	37.360360	1.678166	2.686658	4.700370
	Turkyilmazoglu [6]	37.360360	1.678167	2.686657	4.700370

20	Current – solve_bvp	105.153535	2.366483	3.807546	6.702932
	Mahyuddin et al. [14]	105.153571	2.366480	3.807548	6.702936
	Mustafa et al. [13]	105.153500	2.366480	3.807548	6.702935
	Turkyilmazoglu [6]	105.153500	2.366484	3.807547	6.702932

Table 3 *Verification of the numerical program coding by comparison of numerical results with Mahyuddin et al. [14] for some values of* $\boldsymbol{\phi}$ *when* $\boldsymbol{S_1 = S_2 = 0,\ \lambda = 3, Pr = 6.2}$

Nanoparticle: Copper (Cu)					
ϕ		$-F'(0)$	$G'(0)$	$-\theta(0)$	$-H(\infty)$
0.01	Current – solve_bvp	6.708455	0.978273	4.282608	2.245309
	Mahyuddin et al. [14]	6.708455	0.978273	4.282608	2.245309
0.05	Current – solve_bvp	7.250189	1.057272	3.950165	2.077540
	Mahyuddin et al. [14]	7.250189	1.057272	3.950165	2.077540
0.10	Current – solve_bvp	7.680564	1.120032	3.587596	1.961126
	Mahyuddin et al. [14]	7.680564	1.120032	3.587596	1.961126

3.1 Effects of Stretching Disk (No Slip Condition)

Fig. 2 illustrates the impact of the stretching parameter $0.2 \leq \lambda \leq 2.0$ on the dimensionless functions while other parameters are set as constants such that $\phi = 0.01$; $S_1 = S_2 = 0$, and $Pr = 6.2$. Fig. 2(a)-(c) indicate that the velocity overshoots close to the surface of the stretching disk when the stretching rate is low. The graph of temperature functions, Fig. 2(d), demonstrates the necessity of higher stretching rate to ensure it fulfils the boundary condition at $\eta \to \infty$. It can be observed from Fig. 2(d) that the profiles for $\lambda =$ 0.2 and 0.6 are not valid since they do not approach the far-field condition $\theta \to 0$ asymptotically.

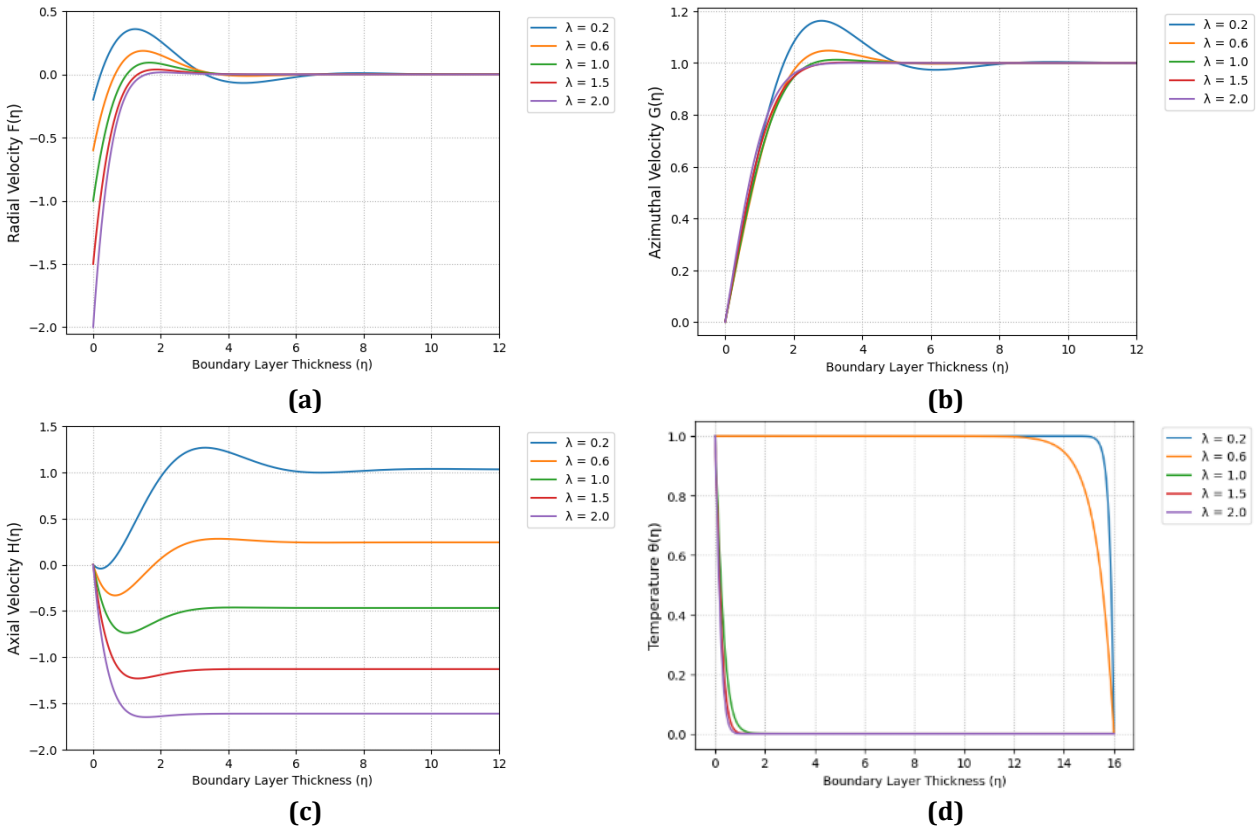

Fig. 2 *Effect of stretching parameter,* $\boldsymbol{\lambda}$ *on dimensionless functions (a)* $F(\eta)$*; (b)* $G(\eta)$*; (c)* $H(\eta)$*; (d)* $\theta(\eta)$*; when* $\phi = 0.01, S_1 = S_2 = 0,$ *and* $Pr = 6.2$

J. of Science and Technology Vol. 16 No. 2 (2024) p. 85-95

3.2 Effects of Thermal Slip and Velocity Slip

Next, the influence of thermal slip S_2 is investigated while keeping the velocity slip constant at $S_1 = 0.3$. Thermal slip values within the range $0.1 \leq S_2 \leq 0.5$ are considered in the numerical computations. Since our aim is to examine the effect of thermal slip along with the presence of velocity slip and stretching, hence λ is first set to 0.5. Visual inspection on the temperature function shown in Fig. 3 indicates that a larger value of stretching parameter is needed to counteract the effect of thermal slip in obtaining physical plausible temperature profile that meets the boundary conditions. This led to a significant finding that a larger stretching rate is necessary to obtain physically realistic similarity solution. Hence, the value of $\lambda = 1.2$ is used as it provides a meaningful temperature profile across different thermal slip values, see Fig. 4(d). Observations of the dimensionless velocity functions (Figs. 4(a)-(c)) shows that they shared very similar behaviour across different values of thermal slip.

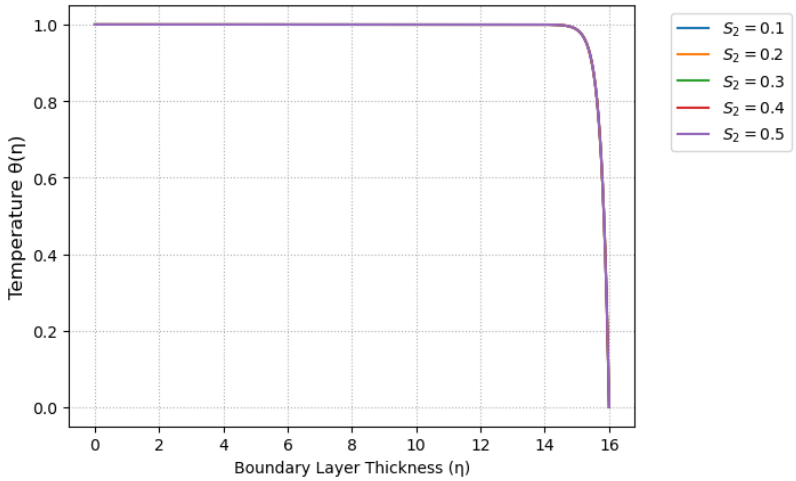

Fig. 3 *Variation of thermal slip parameter S_2 to obtain meaningful solutions temperature with $\phi = 0.01$, $S_1 = 0.3, \lambda = 0.5$ and $Pr = 6.2$*

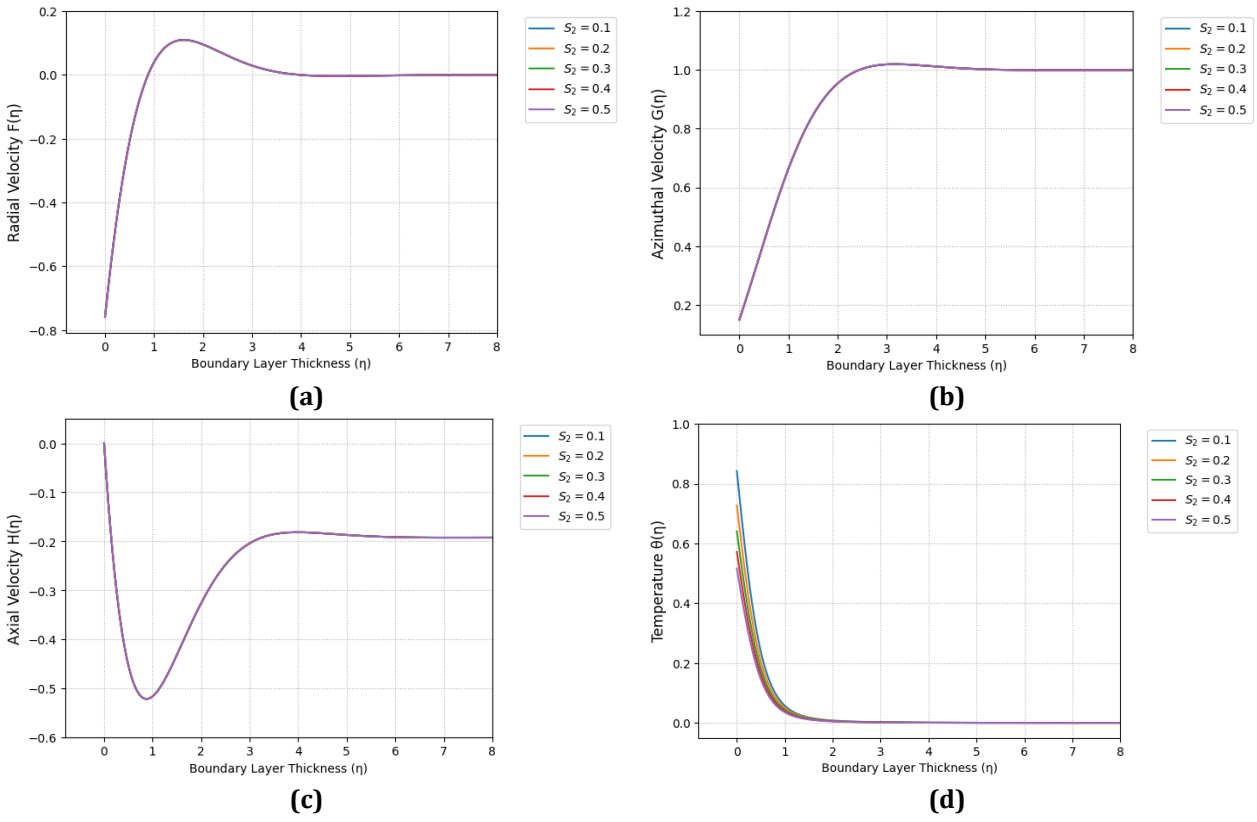

Fig. 4 *Change in of thermal slip parameter S_2 affects dimensionless functions (a) $F(\eta)$; (b) $G(\eta)$; (c) $H(\eta)$; (d) $\theta(\eta)$; with $\phi = 0.01$, $S_1 = 0.3$, $\lambda = 1.2$ and $Pr = 6.2$*

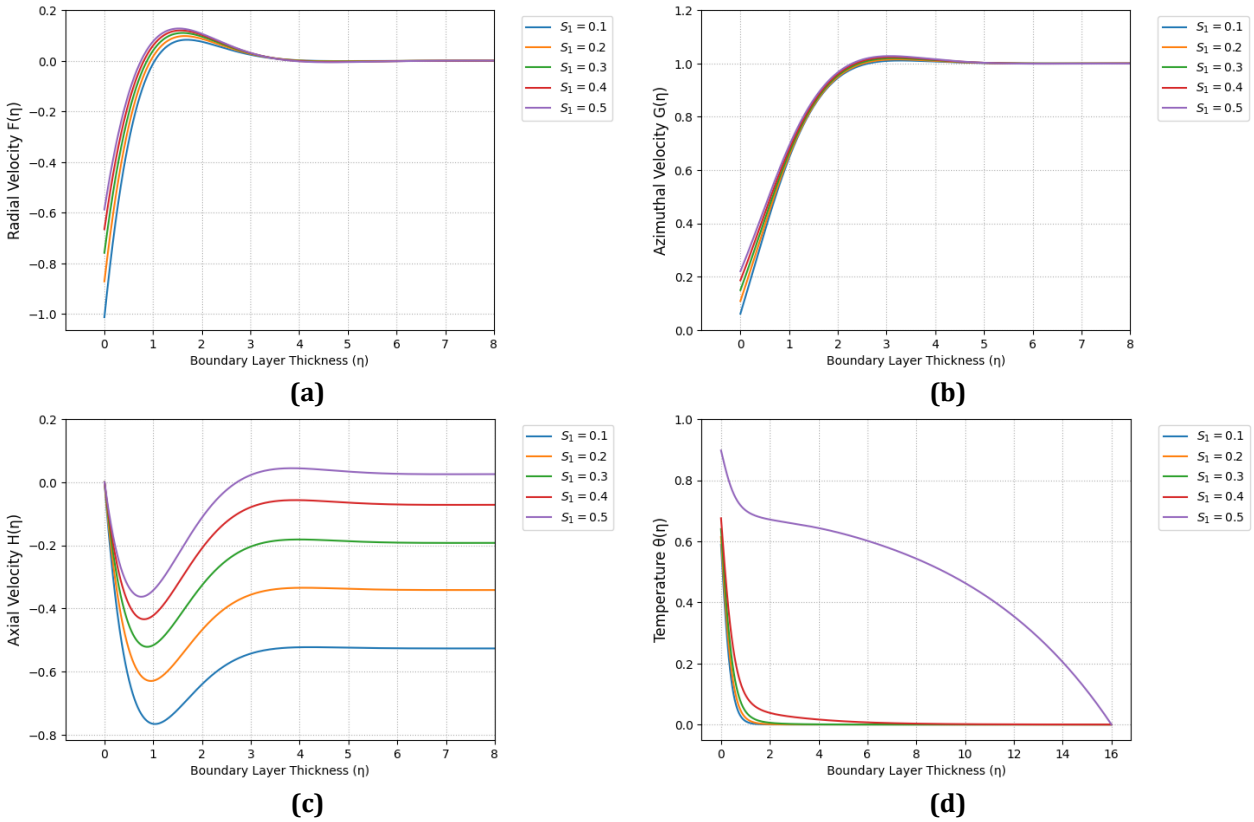

Fig. 5 *Change in velocity slip parameter S_1 affects dimensionless functions (a) $F(\eta)$; (b) $G(\eta)$; (c) $H(\eta)$; (d) $\theta(\eta)$ with $\phi = 0.01$, $S_2 = 0.3$, $\lambda = 1.2$ and $Pr = 6.2$*

Additionally, the dimensions of different profiles are analysed for varying velocity slip values, while thermal slip and stretching parameter remain constant. In contrast to thermal slip, velocity slip significantly affects the radial, azimuthal, and axial velocity profiles, as shown in Fig. 5(a)-(c). However, a prominent effect is observed on the axial velocity, Fig. 5(c). The axial velocity decreases to its lowest point near the stretching disk, then rises to match the outer flow velocity in the far-field condition. From Fig. 5(d), it is observed that a relatively large value of velocity slip ($S_1 = 0.5$), even using a large stretching value, say, $\lambda = 1.2$, obtaining a temperature profile that meets the boundary conditions in a physically plausible way is not possible. In this case, velocity slip must be less than 0.4 in order to satisfy the boundary conditions of the temperature function.

3.3 Local Skin Friction Coefficient and Local Nusselt Number

Fig. 6 illustrates the plots of local skin friction coefficient, $Re_r^{1/2}\, C_f$ versus λ for various volume fractions of nanoparticle, velocity slip, and thermal slip. Two different kinds of nanoparticles, Cu and TiO_2, are considered. An increase in the volume fraction of nanoparticles resulted in a noticeable change in the variation of the local skin friction coefficient when velocity slip and thermal slip were both set to zero. When slip conditions are present, the local skin friction coefficient is lower compared to the no-slip case. However, this coefficient increases with an increased percentage of nanoparticles as the stretching parameter increases, while the velocity slip and thermal slip remain constant. When greater values of velocity slip and thermal slip are taken into account, the local skin friction coefficient is notably lower than in previous cases. Despite having a greater concentration of nanoparticles, the higher slip values impede the rise in the local skin friction coefficient. For no slip condition, copper has a higher value than titanium dioxide when 10% ($\phi = 0.1$) volume fraction of nanoparticle is being used. However, with slip conditions present, the difference between the two nanoparticles becomes insignificant.

Next, Fig. 7 depicts the variation of local Nusselt number, $Re_r^{-1/2}\, Nu_r$ against λ for different values of volume fractions of nanoparticle, velocity slip, and thermal slip for TiO_2 and Cu nanoparticles. In the absence of slip conditions, the local Nusselt number increases as the stretching parameter is increased. Utilizing a larger volume fraction of nanoparticles (10%) maximizes the rate of heat transfer compared to using a 1% volume fraction of nanoparticles. Under slip conditions, the local Nusselt number is notably lower compared to the no-slip scenario. When both velocity slip and thermal slip parameters are set to 0.1, a higher volume fraction of nanoparticles (10%) leads to a slight improvement in the rate of heat transfer as the stretching parameter increases. However,

J. of Science and Technology Vol. 16 No. 2 (2024) p. 85-95

when there are increased levels of velocity slip and thermal slip, paired with a higher concentration of nanoparticles, the rate of heat transfer is further diminished, as illustrated in Fig. 7. For both no slip and slip condition, there is only marginal difference between the two nanoparticles. Hence, it can be concluded that switching from TiO_2 to Cu does not result in a notable enhancement in the heat transfer speed when combined with the primary fluid.

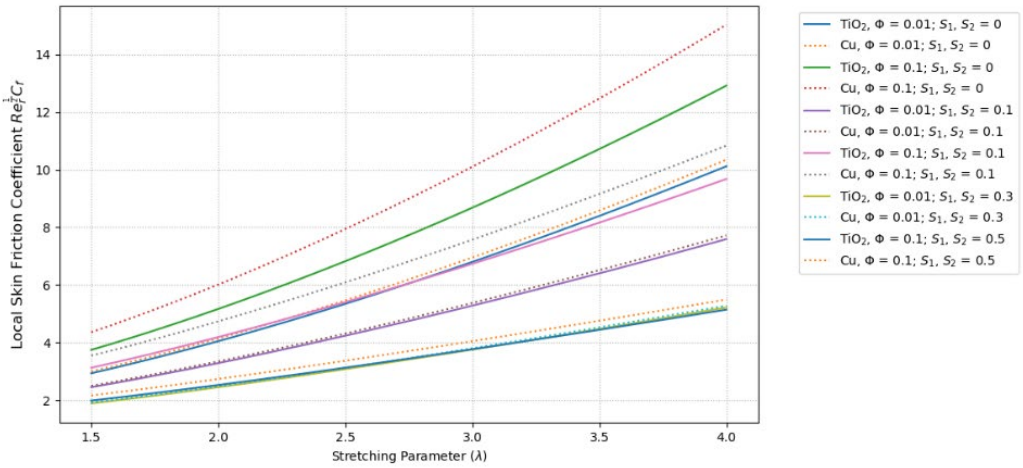

Fig. 6 *Different values of ϕ, S_1, and S_2 results in variation of local skin friction coefficient, $Re_r^{1/2}C_f$ against λ when $Pr = 6.2$ (TiO_2 and Cu nanoparticle)*

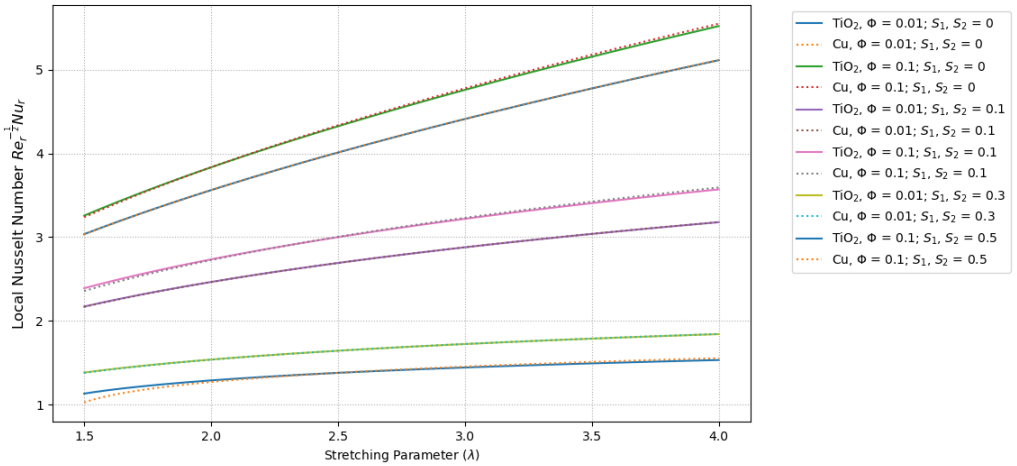

Fig. 7 *Different values of ϕ, S_1, and S_2 results in variation of local Nusselt number, $Re_r^{-1/2}Nu_r$ against λ when $Pr = 6.2$ (TiO_2 and Cu nanoparticle)*

4. Conclusions

This study investigates the heat transfer process in Bödewadt slip flow on nanofluids, considering velocity and thermal slip effects on a stretching disk. Building on previous research, particularly by Mahyuddin et al. [14] and Abbas et al. [15], this study employed Python's solve_bvp module to numerically solved the problem. This work contributes to the mathematical analysis of Bödewadt slip flow on nanofluids, highlighting the effects of velocity and thermal slip over a stretching disk.

The conclusions that can be drawn from this work are:

1. Thermal slip has minimal impact on radial, azimuthal, and axial velocities, which maintain a steady pattern.
2. Velocity slip causes variations in temperature and velocity profiles, with a larger stretching rate required for significant temperature profiles at higher velocity slip values.
3. Heat transfer is enhanced with smaller slip values on the stretching disk, while larger slip values offer no further improvement.

4. Changing the nanoparticle from TiO_2 to Cu does not significantly enhance heat transfer.

Acknowledgement

The authors want to express their gratitude for the technical assistance provided by Universiti Sains Malaysia. The financial assistance under the Fundamental Research Grant Scheme (FRGS) provided by Ministry of Higher Education, Malaysia is also acknowledged. The project code is FRGS/1/2024/STG06/USM/02/10.

Conflict of Interest

All authors confirm that they do not have any conflicts of interest.

Author Contribution

The authors confirm that each part of this work has been equally contributed to. Both authors examined and endorsed the final version of this manuscript.

References

[1] Choi, S. U., & Eastman, J. A. (1995). Enhancing thermal conductivity of fluids with nanoparticles (Rep. No. ANL/MSD/CP-84938; CONF-951135-29). Argonne National Lab., Argonne, IL, USA.
[2] Bödewadt, V. U. (1940). Die drehströmung über festem grunde, ZAMM-Journal of Applied Mathematics and Mechanics/Zeitschrift für Angewandte Mathematik und Mechanik, 20(5), 241–253. https://doi.org/10.1002/zamm.19400200502
[3] Schlichting, H., & Gersten, K. (2017). *Boundary-layer theory (9th ed.)*. SpringerLink.
[4] Rahman, M., & Andersson, H. I. (2017). On heat transfer in Bödewadt flow, *International Journal of Heat and Mass Transfer, 112*, 1057–1061. https://doi.org/10.1016/j.ijheatmasstransfer.2017.05.024
[5] Rafiq, T., & Hashmi, M. M. (2019). Bödewadt flow over a permeable disk with homogeneous-heterogeneous reactions: A numerical study, *Applied Sciences, 9(19)*, 4046. https://doi.org/10.3390/app9194046
[6] Turkyilmazoglu, M. (2015). Bödewadt flow and heat transfer over a stretching stationary disk, *International Journal of Mechanical Sciences, 90*, 246–250. https://doi.org/10.1016/j.ijmecsci.2014.10.022
[7] Sahoo, B., Abbasbandy, S., & Poncet, S. (2014). A brief note on the computation of the Bödewadt flow with Navier slip boundary conditions, *Computers & Fluids, 90*, 133–137. https://doi.org/10.1016/j.compfluid.2013.11.020
[8] Rahman, M., & Andersson, H. I. (2018). Revolving flow of a fluid-particle suspension with suction, *Alexandria Engineering Journal, 57(4)*, 2567–2572. https://doi.org/10.1016/j.aej.2017.08.017
[9] Mustafa, M., Pop, I., Naganthran, K., & Nazar, R. (2018). Entropy generation analysis for radiative heat transfer to Bödewadt slip flow subject to strong wall suction, *European Journal of Mechanics B/Fluids, 72*, 179–188. https://doi.org/10.1016/j.euromechflu.2018.05.010
[10] Sahoo, B. (2011). Effects of slip on steady Bödewadt flow and heat transfer of an electrically conducting non-Newtonian fluid, *Communications in Nonlinear Science and Numerical Simulation, 16(11)*, 4284–4295. https://doi.org/10.1016/j.cnsns.2010.11.023
[11] Sahoo, B., Poncet, S., & Labropulu, F. (2015). Suction/injection effects on the swirling flow of a Reiner-Rivlin fluid near a rough surface, *Journal of Fluids, 2015*, 253504. https://doi.org/10.1155/2015/253504
[12] Sahoo, B., & Shevchuk, I. V. (2019). Heat transfer due to revolving flow of Reiner-Rivlin fluid over a stretchable surface, *Thermal Science and Engineering Progress, 10*, 327–336. https://doi.org/10.1016/j.tsep.2019.03.004
[13] Mustafa, M., Khan, J. A., Hayat, T., & Alsaedi, A. (2015). On Bödewadt flow and heat transfer of nanofluids over a stretching stationary disk, *Journal of Molecular Liquids, 211*, 119–125. https://doi.org/10.1016/j.molliq.2015.06.065
[14] Mahyuddin, A. A., Lok, Y. Y., & Ahmad, S. (2022). Bödewadt flow and heat transfer in nanofluid over a permeable and radially stretching disk, *Sains Malaysiana, 51*, 619–632. http://dx.doi.org/10.17576/jsm-2022-5102-25
[15] Abbas, Z., Siddique, S., Rafiq, M. Y., & Rehman, A. U. (2023). On generalized Bödewadt flow of TiO2/water nanofluid over a permeable surface with temperature jump, *Advances in Mechanical Engineering, 15(10)*. https://doi.org/10.1177/16878132231201299
[16] Joshi, V. K., Ram, P., Sharma, R. K., & Tripathi, D. (2017). Porosity effect on the boundary layer Bodewadt flow of a magnetic nanofluid in the presence of geothermal viscosity, *European Physical Journal Plus, 132*, 254. https://doi.org/10.1140/epjp/i2017-11511-0
[17] Hani, U., Khan, J. A., Rauf, A., Mustafa, F., & Shehzad, S. A. (2022). Bayesian and numerical techniques for non-Newtonian Bödewadt nanofluid flow above a stretchable stationary disk, *Arabian Journal for Science and Engineering, 47*(12), 15931–15945. https://doi.org/10.1007/s13369-022-06773-x

[18] Sunil, S., Garg, D., Joshi, V. K., Sharma, K., & Kumar, S. (2023). Effect of thermal radiation on Bodewadt flow in the presence of porous medium, *Pramana – Journal of Physics, 97*(1), 16. https://doi.org/10.1007/s12043-022-02483-z
[19] Rauf, A., Mushtaq, T., Javed, M., Alahmadi, H., & Shehzad, S. A. (2023). Modeling and analysis of Bödewadt hybrid nanofluid flow triggered by a stretchable stationary disk under Hall current, *Case Studies in Thermal Engineering, 49*, 103315. https://doi.org/10.1016/j.csite.2023.103315
[20] Pandey, A. K., & Das, A. (2024). Thermohydrodynamics of Bödewadt hybrid-nanofluid flow in a horizontal magnetic field, *European Journal of Mechanics B/Fluids, 106*, 148–165. https://doi.org/10.1016/j.euromechflu.2024.04.011
[21] Khan, J. A., Mustafa, M., Hayat, T., & Alzahrani, F. (2017). Numerical study for Bödewadt flow of water-based nanofluid over a deformable disk: Buongiorno model, *Indian Journal of Physics, 91*, 527–533. https://doi.org/10.1007/s12648-017-0959-5
[22] Shakeel, A., & Mustafa, M. (2023). Assessment of Bödewadt flow over a stretchable porous surface with variable physical properties: A comparative study, *Numerical Heat Transfer, Part B: Fundamentals*, 1–14. https://doi.org/10.1080/10407790.2023.2274452
[23] Shafiq, A., Rasool, G., & Khalique, C. M. (2020). Significance of thermal slip and convective boundary conditions in three dimensional rotating Darcy-Forchheimer nanofluid flow, *Symmetry, 12(5)*, 741. https://doi.org/10.3390/sym12050741
[24] Rafiq, T., Mustafa, M., & Khan, J. A. (2019). Numerical study of Bödewadt slip flow on a convectively heated porous disk in a nanofluid, *Physica Scripta, 94(9)*, 095701. https://doi.org/10.1088/1402-4896/ab1549
[25] Çengel, Y., & Cimbala, J. (2018). *Fluid Mechanics: Fundamentals and Applications (4th ed.)*. McGraw-Hill.
[26] Alkuhayli, N. A. M. (2023). Heat transfer analysis of a hybrid nanofluid flow on a rotating disk considering thermal radiation effects, *Case Studies in Thermal Engineering, 49*, 103131. https://doi.org/10.1016/j.csite.2023.103131
[27] The SciPy Community. (2024). scipy.integrate.solve_bvp. SciPy API. https://docs.scipy.org/doc/scipy/reference/generated/scipy.integrate.solve_bvp.html
[28] Andersson, H. I. (2006). Comments on BVPs in non-Newtonian boundary-layer flow, *Applied Mathematics and Computation, 182*(2), 1714–1716. https://doi.org/10.1016/j.amc.2006.06.011
[29] Pantokratoras, A. (2009). A common error made in investigation of boundary layer flows, *Applied Mathematical Modelling, 33*(1), 413–422. https://doi.org/10.1016/j.apm.2007.11.009